

Loss of Pdk1-Foxo1 Signaling in Myeloid Cells Predisposes to Adipose Tissue Inflammation and Insulin Resistance

Yoshinaga Kawano,¹ Jun Nakae,¹ Nobuyuki Watanabe,² Shiho Fujisaka,³ Kristy Iskandar,⁴ Risa Sekioka,¹ Yoshitake Hayashi,⁵ Kazuyuki Tobe,³ Masato Kasuga,⁶ Tetsuo Noda,⁷ Akihiko Yoshimura,⁸ Masafumi Onodera,² and Hiroshi Itoh¹

Chronic inflammation in adipose tissue contributes to obesity-related insulin resistance. The 3-phosphoinositide-dependent protein kinase 1 (Pdk1)/forkhead transcription factor (Foxo1) pathway is important in regulating glucose and energy homeostasis, but little is known about this pathway in adipose tissue macrophages (ATMs). To investigate this, we generated transgenic mice that carried macrophage/granulocyte-specific mutations, including a *Pdk1* knockout (*LysMPdk1*^{-/-}), a *Pdk1* knockout with transactivation-defective Foxo1 ($\Delta 256$ *LysMPdk1*^{-/-}), a constitutively active nuclear (CN) Foxo1 (*CNFoxo1*^{LysM}), or a transactivation-defective Foxo1 ($\Delta 256$ *Foxo1*^{LysM}). We analyzed glucose metabolism and gene expression in ATM populations isolated with fluorescence-activated cell sorting. The *LysMPdk1*^{-/-} mice exhibited elevated M1 macrophages in adipose tissue and insulin resistance. Overexpression of transactivation-defective Foxo1 rescued these phenotypes. *CNFoxo1*^{LysM} promoted transcription of the C-C motif chemokine receptor 2 (*Ccr2*) in ATMs and increased M1 macrophages in adipose tissue. On a high-fat diet, *CNFoxo1*^{LysM} mice exhibited insulin resistance. *Pdk1* deletion or Foxo1 activation in bone marrow-derived macrophages abolished insulin and interleukin-4 induction of genes involved in alternative macrophage activation. Thus, Pdk1 regulated macrophage infiltration by inhibiting Foxo1-induced *Ccr2* expression. This shows that the macrophage Pdk1/Foxo1 pathway is important in regulating insulin sensitivity in vivo. *Diabetes* 61:1935–1948, 2012

Obesity is a predisposing factor for the development of type 2 diabetes, hypertension, hyperlipidemia, and atherosclerosis (1). Chronic activation of intracellular proinflammatory pathways in adipose tissue contributes to obesity-related insulin resistance. Adipose tissue macrophages (ATMs) are a major source of

proinflammatory cytokines, including interleukin (IL)-6, IL-1 β , and tumor necrosis factor (TNF)- α , which can decrease insulin sensitivity in insulin target cells (2). However, only sparse evidence suggests that ATMs may become insulin resistant and play a role in insulin signaling (3–9).

The 3-phosphoinositide-dependent protein kinase 1 (Pdk1)-forkhead transcription factor (Foxo1) signaling pathway regulates energy and glucose metabolism in several insulin-responsive tissues, including pancreatic β -cells and proopiomelanocortin and agouti-related protein neurons (10,11). However, few studies investigate this signaling pathway in ATMs. Recent reports suggest that activation of Foxo1 in macrophages promotes inflammation by inducing IL-1 β expression (12) or toll-like receptor 4-mediated signaling (13). They show that Foxo1 could induce inflammatory cascades, but they do not investigate the role of Foxo1 specifically in ATMs in vivo.

In the current study, we generated transgenic mice that carried macrophage-specific mutations, including a *Pdk1* knockout, a constitutively nuclear (CN) *Foxo1*, or a transactivation-defective *Foxo1*. We analyzed insulin sensitivity in these mice in vivo. We found a novel Pdk1-Foxo1 signaling mechanism that regulated M1 macrophage recruitment.

RESEARCH DESIGN AND METHODS

Mice. All experimental protocols with mice were approved by the animal ethics committees of the Keio University School of Medicine (09134-1). To create macrophage-specific *Pdk1* knockout mice, *Pdk1*^{fllox/fllox} mice (11) were crossed with *LysMCre* transgenic mice (14). The generation of *R26*^{flxneoCNFoxo1} mice was described previously (11). Only animals from the same generation of the mixed-background strain were compared. All mice studied were examined on a B6/129 mixed genetic background. Mice were obtained from two independent cohorts of independent breeders, and littermates were used for every in vivo study. Animals were housed in sterile cages in a barrier animal facility at 22–24°C with a 12-h light/dark cycle.

Antibodies. All antibodies used in the current study are available upon request. **Analytical procedures.** For high-fat diet (HFD) studies, we used age-matched (28-week-old) mice. We started the HFD at age 4 weeks for the 24-week HFD and at age 24 weeks for the 4-week HFD. All of the HFD mice were compared with age-matched mice fed a normal chow diet (NCD). The HFD was described previously (15). Analysis was limited to male mice because they are more susceptible to insulin resistance and diabetes. We performed intraperitoneal glucose tolerance tests (IPGTTs) after an overnight fast and insulin tolerance tests (ITTs) after fasting for 3–5 h. The area under the curve (AUC) was calculated from the level of each measured point by the trapezoidal method.

Flow cytometric analysis. Flow cytometric analysis was performed as described previously (16).

Hepatic glycogen content. We measured glycogen content as described previously (17).

Immunofluorescence. Double-positive cells were counted and marked digitally to prevent multiple counts with Adobe Photoshop CS4 EXTENDED and ImageJ software (National Institutes of Health, Bethesda, MD). Cells were counted in eight mice for each HFD duration. At least 300 cells were counted in each mouse.

From ¹Frontier Medicine on Metabolic Syndrome, Division of Endocrinology, Metabolism, and Nephrology, Department of Internal Medicine, Keio University School of Medicine, Tokyo, Japan; the ²Department of Human Genetics, National Center for Child Health and Development, Tokyo, Japan; the ³Department of Internal Medicine, University of Toyama, Toyama, Japan; the ⁴Pediatric Research Office, Department of Child Health, Faculty of Medicine, Universitas Gadjah Mada, Sardjito Hospital, Yogyakarta, Indonesia; the ⁵Division of Molecular Medicine and Medical Genetics, International Center for Medical Research and Treatment, Kobe University Graduate School of Medicine, Kobe, Japan; the ⁶Research Institute, International Medical Center of Japan, Tokyo, Japan; the ⁷Department of Cell Biology, Japanese Foundation for Cancer Research, Cancer Institute, Tokyo, Japan; and the ⁸Department of Microbiology and Immunology, Keio University School of Medicine, Tokyo, Japan.

Corresponding author: Jun Nakae, jnakae35@sc.itc.keio.ac.jp.

Received 6 June 2011 and accepted 6 March 2012.

DOI: 10.2337/db11-0770

This article contains Supplementary Data online at <http://diabetes.diabetesjournals.org/lookup/suppl/doi:10.2337/db11-0770/-/DC1>.

© 2012 by the American Diabetes Association. Readers may use this article as long as the work is properly cited, the use is educational and not for profit, and the work is not altered. See <http://creativecommons.org/licenses/by-nc-nd/3.0/> for details.

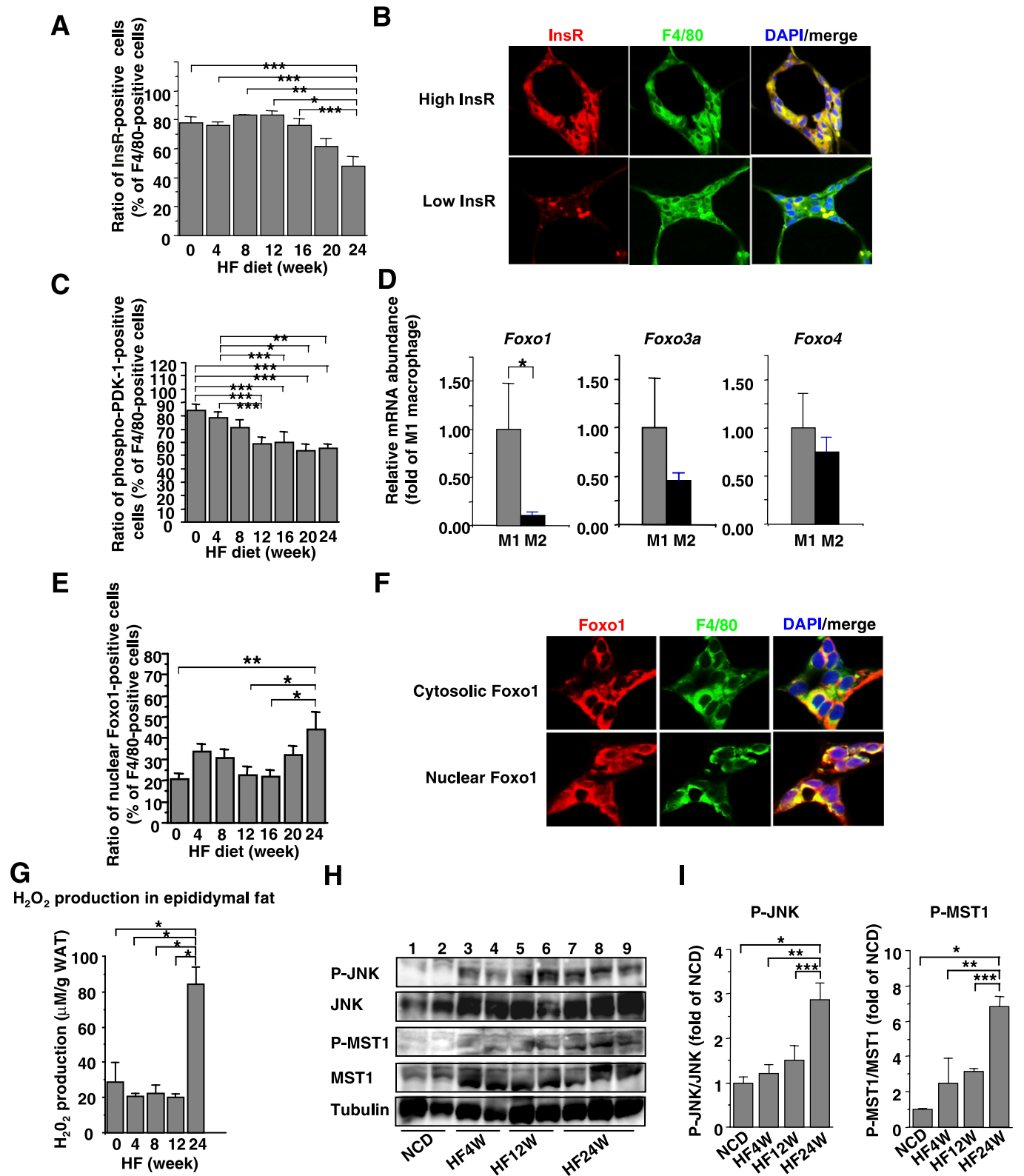


FIG. 1. Characterization of InsR, Pdk1, and Foxo1 in ATMs during an HFD. **A:** The percentages of InsR⁺ cells among F4/80⁺ cells in epididymal fat from age-matched wild-type mice fed an NCD and 24 weeks of an HFD. Values are means + SEM of eight mice. **P* < 0.005, ***P* < 0.01, and ****P* < 0.05 (one-factor ANOVA). **B:** Representative immunofluorescence images of epididymal fat double labeled for InsR and F4/80 in wild-type mice fed an HFD for 24 weeks. Cells that exhibit high expression level of InsR protein (*top*); cells that exhibit low or faint expression level of InsR (*bottom*). Red, green, and blue indicate InsR, F4/80, and DAPI staining, respectively. **C:** The percentages of phospho-PDK1⁺ cells among F4/80⁺ cells in epididymal fat from age-matched wild-type mice fed an NCD and 24 weeks of an HFD. Values are means + SEM of eight mice. **P* < 0.005, ***P* < 0.01, ****P* < 0.05 (one-factor ANOVA). **D:** Real-time PCR analysis of *Foxo* family members in cell populations sorted by flow cytometry analysis of the SVF from the epididymal fats of wild-type mice fed an HFD for 16 weeks, using anti-F4/80, anti-CD11c, and anti-CD206 antibodies. The levels of each transcript were normalized to the level in M1 macrophages. Values are means + SEM of three mice. **P* < 0.05 (one-factor ANOVA, M1 vs. M2 macrophages). **E:** The percentages of nuclear Foxo1⁺ cells among F4/80⁺ cells in the epididymal fat of age-matched wild-type

H₂O₂ production. Measurement of H₂O₂ production was performed as described elsewhere (18). Epididymal fat was dissected from age-matched male C57BL/6J mice on either an NCD or a 4-24 week HFD.

Counting crown-like structures. Measurement of number of crown-like structures (CLSs) was performed as described previously (16).

Cell size measurements. Adipocyte size was measured with FLVFS-LS software (Flovel, Tokyo, Japan) by manually tracing a minimum of 1,200 adipocytes for each mouse. We measured adipocytes in at least six mice of each genotype.

Isolation of murine bone marrow-derived macrophages. Isolation of bone marrow-derived macrophages (BMDMs) was performed as described elsewhere (19).

Transwell migration assay. Transwell migration assays were performed as previously described (20).

Viral transduction. Adenovirus constructs that encoded Foxo1 mutants are described elsewhere (21,22). RAW264.7 cells were infected with adenoviruses (10–100 multiplicity of infection [MOI]) and harvested after 48 h. For cotransductions, cells were first transduced with an adenovirus that encoded Flag-CNFoxo1 at the indicated MOI for 8 h. The virus was then removed from the culture dish, and the cells were transduced with another adenovirus that encoded HA-Δ256Foxo1 at the indicated MOI for 8 h.

RNA isolation and real-time PCR. The isolation of total RNA and real-time PCR were performed as described previously (15). All primer sequences are available upon request.

Western blotting. Western blotting was performed as described previously (15). Insulin-stimulated phosphorylation of insulin receptor substrates (IRSs) and Akt were performed as described elsewhere (23).

Construction of C-C motif chemokine receptor 2 promoter-directed luciferase reporter vectors. Several DNA fragments containing the mouse C-C motif chemokine receptor 2 (*Ccr2*) promoter were PCR-amplified from mouse genomic DNA. After verifying their nucleotide sequences by DNA sequencing, the *Ccr2* promoter fragments were cloned into the luciferase reporter pGL3-Basic vector (Promega, Madison, WI). All primer sequences are available upon request.

Site-directed mutagenesis. The QuickChange II site-directed mutagenesis kit (Stratagene, La Jolla, CA) was used to alter the consensus Foxo1 binding elements in the *Ccr2* promoter in pGL3-Basic vectors. Mutated nucleotides were confirmed with DNA sequencing. All primer sequences are available upon request.

Luciferase assay. The luciferase assay was performed as described previously (22).

Electrophoretic mobility shift assay. Electrophoretic mobility shift assay (EMSA) and the super shift assay were performed as described previously (24).

Chromatin immunoprecipitation assay. Chromatin immunoprecipitation (ChIP) assay was performed as described previously (22).

Statistical analysis. We calculated descriptive statistics with ANOVA followed by Fisher test (Statview; SAS Institute Inc.). $P < 0.05$ was considered significant. Differences between two groups or among three groups were investigated with two-way repeated-measures ANOVA with an ad hoc multiple comparison method (Fisher least significant differences [LSD] test).

RESULTS

Insulin receptor expression and Pdk1 phosphorylation in ATMs during an HFD. To explore the significance of insulin signaling pathway in ATM, we examined insulin receptor (InsR) protein expression in ATMs by double immunofluorescence with anti-InsR and anti-F4/80 antibodies. During the HFD, ATM InsR protein levels were significantly reduced by ~50% compared with controls (Fig. 1A and B).

Next, we explored Pdk1 expression in ATMs under different diets. Immunofluorescence of epididymal fat from C57BL/6J mice on an HFD for 16 weeks revealed that cells positive for the macrophage marker CD68 were also positive

for Pdk1 (Fig. 2A, top). Because Pdk1 activity depends on Ser 241 phosphorylation (25), we probed with an antiphospho-Pdk1 antibody. On an NCD, ~80% of F4/80⁺ cells were stained with antiphospho-Pdk1. On an HFD for 24 weeks, the proportion of phospho-Pdk1⁺ ATMs gradually decreased from 80% to from 40 to 50% (Fig. 1C). These data confirm that the InsR-Pdk1 pathway was functionally regulated in ATMs during the HFD.

Foxo1 in ATMs under an HFD. To explore the relative importance of Foxo family members in ATMs, we compared the expression of *Foxo1*, *Foxo3a*, and *Foxo4* in M1 and M2 macrophages isolated from the stromal vascular fraction (SVF) of epididymal fat from C57BL/6J mice fed an HFD for 16 weeks. We defined F4/80⁺CD11c⁺CD206⁻ cells as M1 macrophages and F4/80⁺CD11c⁻CD206⁺ cells as M2 macrophages (16). M1 macrophages showed significantly increased *Foxo1* expression compared with M2 macrophages. *Foxo3a* expression was also increased in M1 compared with M2 macrophages but not significantly. In contrast, M1 and M2 macrophages showed similar *Foxo4* expression (Fig. 1D). These observations suggest that Foxo1 played an essential role in ATMs.

Because Foxo1 activity depends on its subcellular localization (26), we examined Foxo1 with immunofluorescence in ATMs from age-matched C57BL/6J mice fed an NCD or HFD. Under the NCD, ~20% of Foxo1 was localized to the nucleus. After 24 weeks of an HFD, ~45% of Foxo1 was localized to the nucleus (Fig. 1E and F). These data suggest that Foxo1 was functionally significant in ATMs.

Foxo1 is regulated by oxidative stress through H₂O₂ production and the Jun NH₂-terminal kinase (JNK)-mammalian Ste20-like kinase 1 (MST1) pathway, which induces Foxo1 nuclear translocation (27–30). The production of H₂O₂ significantly increased at ~24 weeks of HFD (Fig. 1G). Furthermore, JNK and MST1 phosphorylation significantly increased after 24 weeks of HFD (Fig. 1H and I). These data suggest that both decreased Pdk1 phosphorylation and activation of the JNK-MST1 pathway may contribute to Foxo1 nuclear localization.

Deletion of Pdk1 in ATMs causes insulin resistance with rescue by transactivation-defective Foxo1. To clarify the function of Pdk1 in ATMs, we generated mice that lacked *Pdk1* in macrophages/granulocytes (*LysMPdk1*^{-/-}). Efficient, specific *Pdk1* deletion was evidenced by immunofluorescence (Fig. 2A) and Western blot analysis (Fig. 2B). Thus, we could study the effects of cell-specific *Pdk1* deficiency.

The deletion of *Pdk1* in ATMs was expected to cause nuclear localization of Foxo1. Immunofluorescence with an anti-Foxo1 antibody in epididymal fat revealed that ~60–70% of Foxo1 was localized to the nuclei of ATMs in *LysMPdk1*^{-/-} mice (Fig. 2C). We assumed that Foxo1 was active in *Pdk1*-deficient ATMs and that this activity could be blocked with the dominant-negative form of Foxo1 (Δ256Foxo1), which lacked a COOH-terminal transactivation domain (31). To investigate this, we crossed

mice fed an NCD and 24 weeks of an HFD. Values are means + SEM of eight mice. * $P < 0.001$, ** $P < 0.005$ (one-factor ANOVA). F: Representative immunofluorescence images of epididymal fat double labeled for Foxo1 and F4/80 in wild-type mice fed an HFD for 24 weeks. Cytosolic (top) and nuclear Foxo1 (bottom). Red, green, and blue indicate Foxo1, F4/80, and DAPI staining, respectively. G: The release of H₂O₂ from epididymal fats from age-matched male C57BL/6J mice fed an NCD or 4–24 weeks of an HFD. Values are expressed as mean ± SEM of five mice in each condition. * $P < 0.001$ (one-factor ANOVA). H: Western blotting of epididymal fats from age-matched male C57BL/6J mice fed an NCD or 4–24 weeks of an HFD. After transference to nylon membrane, tissue lysates (200 μg) were blotted to the indicated antibodies. I: Quantitative analysis of JNK and MST1 phosphorylation in epididymal fats. The intensity of each band was measured using NIH Image 1.62, and the intensities of bands of phospho-JNK or phospho-MST1 bands were corrected by total JNK or MST1 and calculated as the fold change from NCD. Data are means + SEM of five mice in each genotype. * $P < 0.001$, ** $P < 0.005$, and *** $P < 0.05$ (one-factor ANOVA of NCD vs. HFD). WAT, white adipose tissue; P, phospho; W, weeks. (A high-quality digital representation of this figure is available in the online issue.)

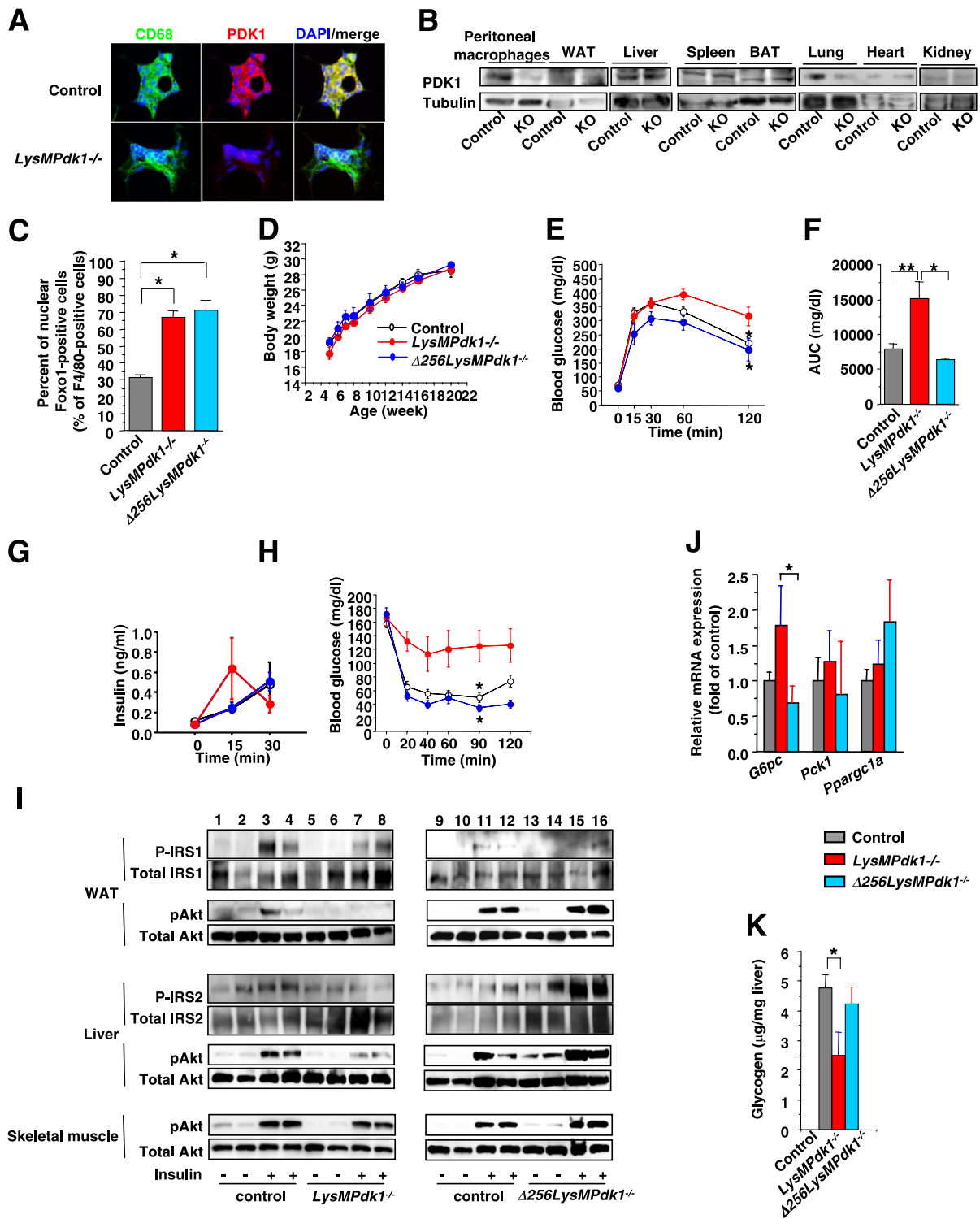


FIG. 2. Effects of the deletion of *Pdk1* or inhibition of the transactivation of Foxo1 on glucose metabolism and insulin sensitivity. **A:** Representative immunofluorescence images of epididymal fat double labeled for CD68 and PDK1 in 24-week-old wild-type and *LysMPdk1^{-/-}* mice. Green, red, and blue indicate CD68, PDK1, and DAPI staining, respectively. **B:** Expression of Pdk1 in peritoneal macrophages and peripheral tissues. Western blot of Pdk1 and tubulin (loading control) in the white adipose tissue (WAT), liver, spleen, brown adipose tissue (BAT), lungs, heart, and kidneys of control and *LysMPdk1^{-/-}* (KO) mice. **C:** The percentages of nuclear Foxo1⁺ among F4/80⁺ cells in epididymal fat of control, *LysMPdk1^{-/-}*, and $\Delta 256LysMPdk1^{+/+}$ mice aged 20–24 weeks. Counting of cells stained with anti-F4/80 and anti-FOXO1 are described in RESEARCH DESIGN AND METHODS. Values are means \pm SEM of three mice in each genotype. **P* < 0.005 (one-factor ANOVA). **D:** Body weight of control, *LysMPdk1^{-/-}*, and $\Delta 256LysMPdk1^{+/+}$ fed an NCD. Data are means \pm SEM of 18–20 mice in each genotype. **E:** IPGTT of control (open circle), *LysMPdk1^{-/-}* (red circle), and $\Delta 256LysMPdk1^{+/+}$ (blue circle) mice fed an NCD. Data are means \pm SEM of 20–25 mice in each genotype at age 20–24 weeks. **P* < 0.05 (two-way repeated-measures ANOVA with an ad hoc multiple comparison method [Fisher LSD test] of *LysMPdk1^{-/-}* vs. control or $\Delta 256LysMPdk1^{+/+}$ mice). **F:** Comparison of AUC in control, *LysMPdk1^{-/-}*, and $\Delta 256LysMPdk1^{+/+}$ mice during IPGTT. Data are means \pm SEM of 20–25 mice in each genotype. **P* < 0.01 (two-way repeated-measures ANOVA with Fisher LSD test of *LysMPdk1^{-/-}* vs. $\Delta 256LysMPdk1^{+/+}$ mice) and ***P* < 0.05 (two-way repeated-measures ANOVA with Fisher LSD test of *LysMPdk1^{-/-}* vs. control mice). **G** and **H:** Insulin secretion (**G**) of control (open circle), *LysMPdk1^{-/-}* (red circle), and $\Delta 256LysMPdk1^{+/+}$ (blue circle) mice during IPGTT and blood glucose (**H**) during ITT. Data are

R26^{flx;neo}Δ256FoxO1 (11) with *LysMCre* transgenic mice to generate *R26^{flx;neo}Δ256FoxO1 LysMCre* ($\Delta256FoxO1^{LysM}$) double heterozygotes. Real-time PCR analysis and immunofluorescence confirmed the macrophage-specific expression of the transgene and the nuclear localization of FLAG- $\Delta256FoxO1$, respectively (Supplementary Figs. 1 and 2). We crossed $\Delta256FoxO1^{LysM}$ with *Pdk1^{flx/+}* to generate double mutant mice ($\Delta256FoxO1^{LysM}Pdk1^{+/-}$). Finally, these mice were crossed with *Pdk1^{flx/+}* to generate $\Delta256FoxO1^{LysM}Pdk1^{-/-}$ ($\Delta256LysMPdk1^{-/-}$) mice (Supplementary Fig. 3). As expected, $\Delta256LysMPdk1^{-/-}$ mice showed excess nuclear Foxo1 in F4/80⁺ cells from epididymal fat (Fig. 2C).

The *LysMPdk1^{-/-}* and $\Delta256LysMPdk1^{-/-}$ mice exhibited normal body weight when fed an NCD (Fig. 2D), and their epididymal fat tissue weight and adipocyte sizes were similar to those of control mice (Supplementary Fig. 4A and B). However, the IPGTTs revealed that *LysMPdk1^{-/-}*, but not $\Delta256LysMPdk1^{-/-}$, mice exhibited glucose intolerance (Fig. 2E and F). Insulin secretion during the IPGTT was higher in *LysMPdk1^{-/-}* mice than in controls and $\Delta256LysMPdk1^{-/-}$ mice, but the difference was not significant (Fig. 2G). Furthermore, insulin tolerance significantly decreased in *LysMPdk1^{-/-}* mice compared with control and $\Delta256LysMPdk1^{-/-}$ mice (Fig. 2H). These data indicate that the deletion of *Pdk1* deteriorates insulin sensitivity and that the ectopic expression of $\Delta256FoxO1$ ameliorates insulin sensitivity.

To identify the tissues that are responsible for insulin resistance, we investigated insulin-stimulated phosphorylation of IRS1, IRS2, and/or Akt in epididymal fats, liver, and skeletal muscle from control, *LysMPdk1^{-/-}*, and $\Delta256LysMPdk1^{-/-}$ mice. In epididymal fat and liver, insulin-stimulated phosphorylation of IRS1 or IRS2 and Akt was significantly decreased in *LysMPdk1^{-/-}* mice compared with control mice (Fig. 2I). However, insulin-stimulated phosphorylation of IRS and Akt in epididymal fat and liver from $\Delta256LysMPdk1^{-/-}$ mice was similar to that of control mice (Fig. 2I). The expression of *G6pc* was significantly increased in liver from *LysMPdk1^{-/-}* compared with $\Delta256LysMPdk1^{-/-}$ mice (Fig. 2J); moreover, the hepatic glycogen content of *LysMPdk1^{-/-}* mice was significantly decreased compared with control and $\Delta256LysMPdk1^{-/-}$ mice (Fig. 2K). In contrast, Akt phosphorylation in skeletal muscle from *LysMPdk1^{-/-}* mice was similar to that of control and $\Delta256LysMPdk1^{-/-}$ mice (Fig. 2I). These data indicate that the deletion of *Pdk1* in ATMs led to insulin resistance, mainly in adipose tissue and liver, and that ectopic expression of $\Delta256FoxO1$ ameliorated insulin resistance in those tissues.

Deletion of *Pdk1* caused an increase of M1 macrophages in adipose tissues. A CLS is the accumulation of immune cells around dead adipocytes (32). We found that the number of F4/80⁺ CLSs per field in epididymal fat was significantly higher in *LysMPdk1^{-/-}* mice than in control and $\Delta256LysMPdk1^{-/-}$ mice (Fig. 3A).

The SVF of adipose tissue from 20-week-old mice contained a substantially higher proportion of F4/80⁺ cells in *LysMPdk1^{-/-}* compared with control mice (Fig. 3B and C). Analysis of macrophage subpopulations in the SVF showed a higher proportion of F4/80⁺CD11c⁺CD206⁻ cells in *LysMPdk1^{-/-}* mice than in control mice (Fig. 3B and C). In contrast, the adipose tissue of $\Delta256LysMPdk1^{-/-}$ mice showed significantly reduced proportions of F4/80⁺ cells and F4/80⁺CD11c⁺CD206⁻ cells compared with *LysMPdk1^{-/-}* mice (Fig. 3B and C). These data suggest that the deletion of *Pdk1* caused a significant increase in the proportion of M1 macrophages in epididymal fat, and the proportion was reduced with the overexpression of $\Delta256FoxO1$.

Consistent with the above findings, the expression of chemokine (C-C motif) ligand 2 (*Ccl2*) (also known as monocyte chemoattractant protein-1 [*Mcp-1*]) and *Cd68* in epididymal fat (Fig. 3D) and of *Ccr2* and *Tnfa* in SVF from *LysMPdk1^{-/-}* mice were significantly increased compared with control and $\Delta256LysMPdk1^{-/-}$ mice (Fig. 3E). Furthermore, the expression level of IL-1 receptor antagonist, which is a naturally occurring antagonist of IL-1 β and produced by adipose and other tissues (33), in SVF from *LysMPdk1^{-/-}* mice was significantly decreased compared with control mice (Fig. 3E). These data support the notion that the deletion of *Pdk1* increased the recruitment of M1 macrophages to adipose tissues.

Macrophage-specific CNFoxo1 transgenic (*CNFoxo1^{LysM}*) mice exhibited insulin resistance. To clarify the function of Foxo1 in ATMs, we generated macrophage-specific CNFoxo1 transgenic mice. We crossed *Rosa26-CNFoxo1* (11) with *LysMCre* (*CNFoxo1^{LysM}*) mice. Real-time PCR revealed that the transgene was expressed exclusively in the spleen, liver, hypothalamus, and lung and in ATMs from the epididymal fat (Supplementary Fig. 5). These tissues have tissue-specific macrophages, which include the cells in the sinusoidal lining of the spleen, Kupffer cells in the liver, microglia in the hypothalamus, and alveolar macrophages in the lung (14,34,35). Therefore, resident macrophages likely account for the increased expression of the transgene in these tissues. Immunofluorescence of the epididymal fat showed that FLAG-CNFoxo1 was exclusively localized in the nucleus of F4/80⁺ macrophages (Supplementary Fig. 6). Furthermore, immunofluorescence revealed that ~50% of F4/80⁺ cells in epididymal fat of *CNFoxo1^{LysM}* mice were positive for FLAG (Fig. 4A) and that the percentages of nuclear Foxo1⁺ cells in adipose tissue of *CNFoxo1^{LysM}* fed an HFD for 16 weeks was significantly increased compared with control mice fed an HFD or *CNFoxo1^{LysM}* fed an NCD (Fig. 4B). These results show that *CNFoxo1^{LysM}* mice were an appropriate model for studying the specific effects of overexpressing Foxo1 in ATMs.

On an NCD, *CNFoxo1^{LysM}* mice exhibited normal body weight, glucose tolerance, insulin secretion, and insulin sensitivity (Supplementary Fig. 7A–D). On an HFD, the body

means \pm SEM of 20–25 mice in each genotype. * $P < 0.05$ (two-way repeated-measures ANOVA with Fisher LSD test of control vs. *LysMPdk1^{-/-}* or $\Delta256LysMPdk1^{-/-}$ mice). I: Insulin-stimulated phosphorylation of IRSs and Akt in epididymal fat (WAT), liver, and skeletal muscle from control, *LysMPdk1^{-/-}*, and $\Delta256LysMPdk1^{-/-}$ mice. For Western blotting with phospho- and total Akt, the same filters, in which tissue lysates (200 μ g) were transferred, were blotted with the indicated antibodies. For immunoprecipitation of IRSs, tissue lysates (10 mg) were immunoprecipitated with the indicated antibodies and blotted with anti-phosphotyrosine antibody and then reblotted with anti-IRS antibody. J: Expression of genes specific for gluconeogenesis in liver from control, *LysMPdk1^{-/-}*, and $\Delta256LysMPdk1^{-/-}$ mice in the random fed state. Values were normalized to β -actin expression and represent means \pm SEM of 8–10 mice in each genotype. * $P < 0.05$ (one-factor ANOVA of *LysMPdk1^{-/-}* vs. $\Delta256LysMPdk1^{-/-}$). K: Hepatic glycogen content. Control ($n = 9$), *LysMPdk1^{-/-}* ($n = 9$), and $\Delta256LysMPdk1^{-/-}$ ($n = 8$) mice were killed in the random fed state for the determination of glycogen levels in liver extracts. Data are means \pm SEM of hepatic glycogen content corrected by the weight of liver per genotype. * $P < 0.05$ (one-factor ANOVA of control vs. *LysMPdk1^{-/-}* mice). (A high-quality digital representation of this figure is available in the online issue.)

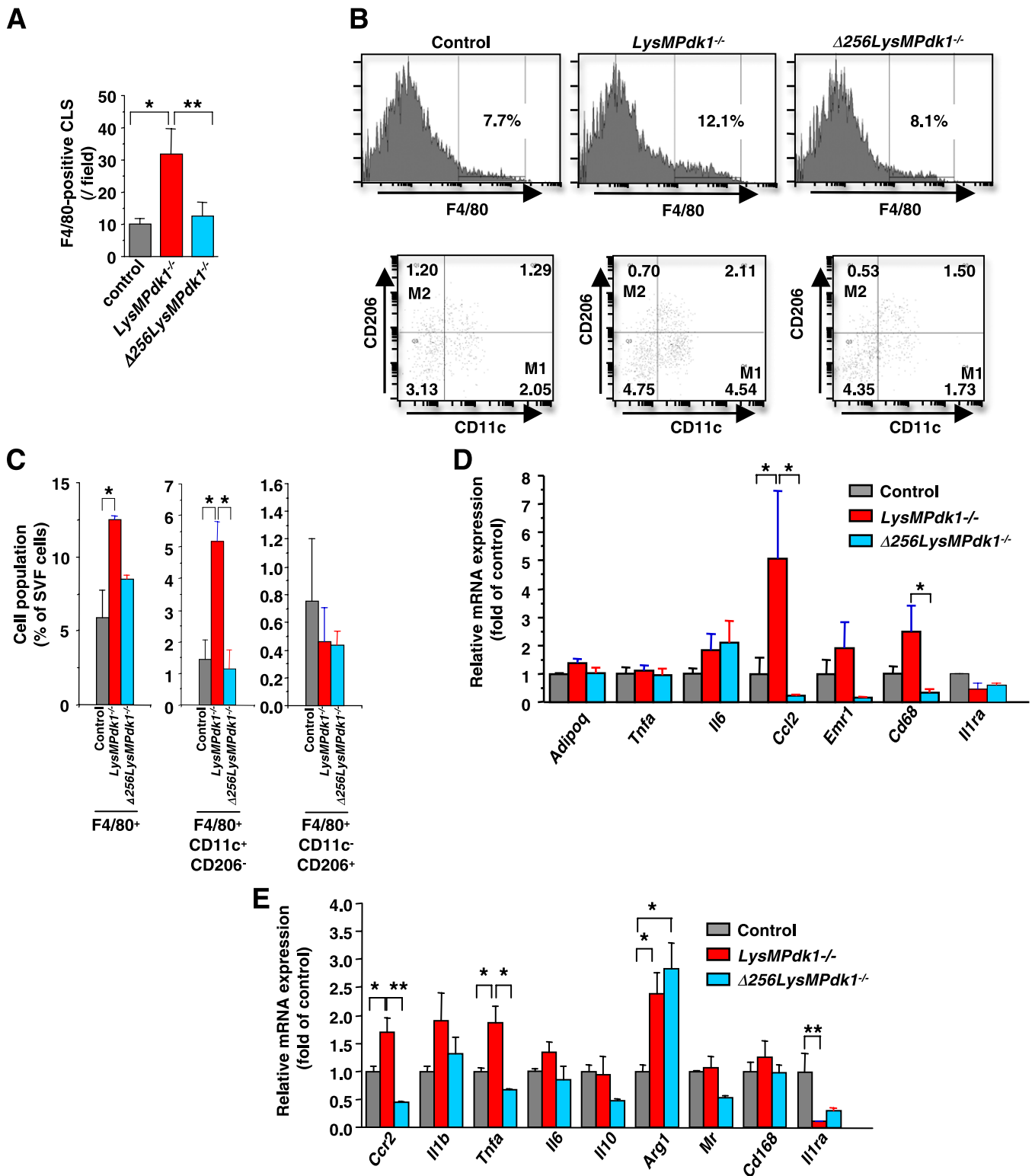


FIG. 3. Effects of *Pdk1* deletion or inhibition of the transactivation of Foxo1 on adipose tissue inflammation. **A:** CLSs in epididymal fats were quantified from eight different fields per mouse and presented as number of CLSs per field. Data are means + SEM of 9–10 mice in each genotype. * $P < 0.01$ (one-factor ANOVA of *LysMPdk1*^{-/-} vs. control mice) and ** $P < 0.05$ (one-factor ANOVA of *LysMPdk1*^{-/-} vs. $\Delta 256$ *LysMPdk1*^{-/-} mice). **B:** The expression of F4/80 and CD11c and CD206 in the SVF of epididymal fat from 20- to 24-week-old mice of the indicated genotype as assessed by flow cytometry. **C:** The percentages of F4/80⁺, F4/80⁺CD11c⁺CD206⁻, and F4/80⁺CD11c⁻CD206⁺ cells within the viable SVF from 20- to 24-week-old mice of control, *LysMPdk1*^{-/-}, and $\Delta 256$ *LysMPdk1*^{-/-} mice. Data are means + SEM of three mice in each genotype analyzed in three independent experiments. * $P < 0.05$ (one-factor ANOVA of *LysMPdk1*^{-/-} vs. control or $\Delta 256$ *LysMPdk1*^{-/-} mice). **D:** Expression of genes in the epididymal fat of control, *LysMPdk1*^{-/-}, and $\Delta 256$ *LysMPdk1*^{-/-} mice. Values were normalized to β -actin expression and represent the means + SEM of 8–10 mice per genotype. * $P < 0.05$ (one-factor ANOVA). **E:** Expression of genes specific for M1 (*Ccr2*, *Il1b*, *Tnfa*, and *Il6*) or M2 (*Il10*, *Arg1*, *Mr*, and *Ccl68*) macrophage in SVF of epididymal fat in control, *LysMPdk1*^{-/-}, and $\Delta 256$ *LysMPdk1*^{-/-} mice. Values were normalized to β -actin expression and represent the means + SEM of 8–10 mice per genotype. * $P < 0.05$ and ** $P < 0.01$ (one-factor ANOVA).

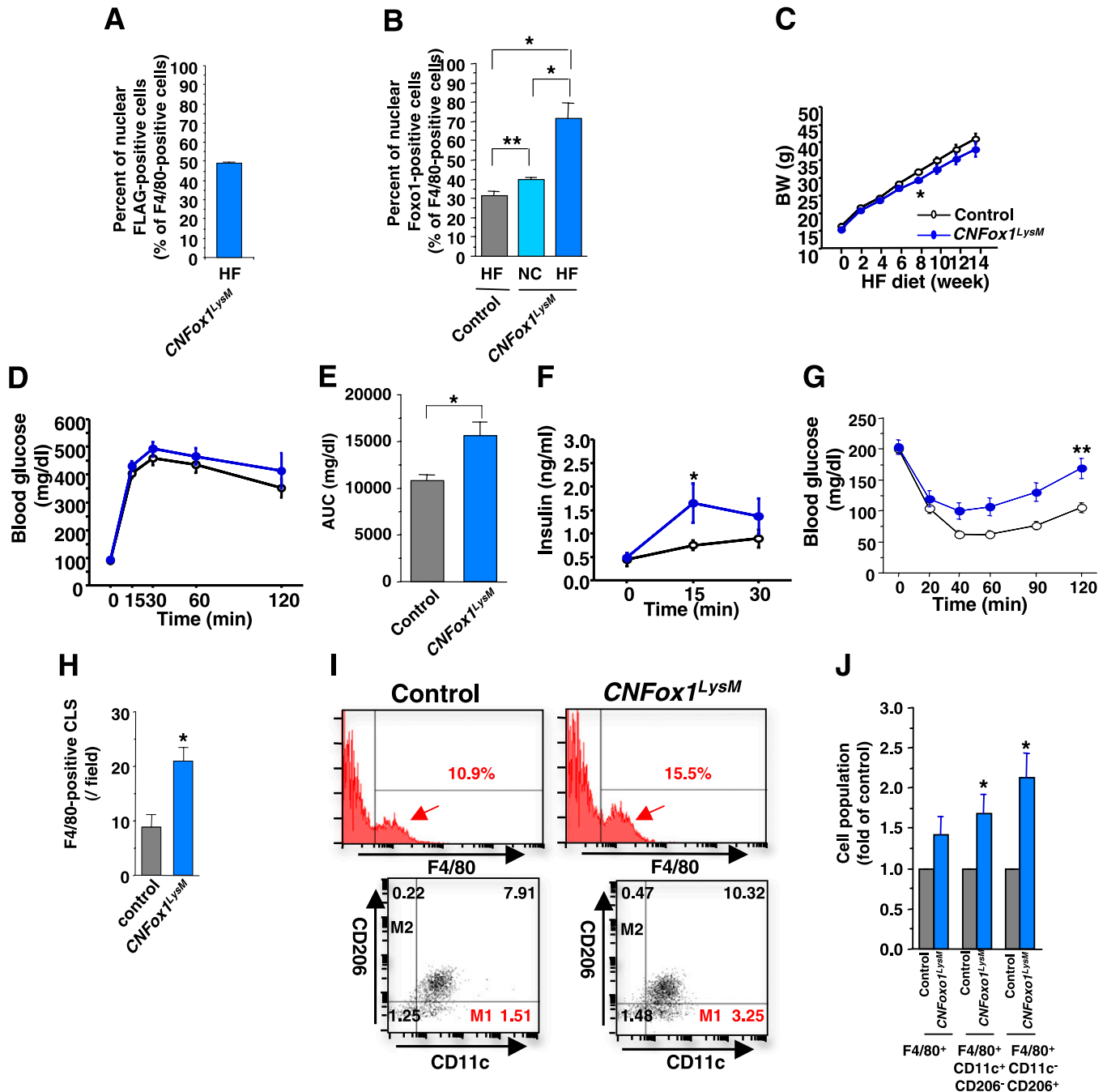


FIG. 4. Effects of the overexpression of CNFoxo1 in macrophages on glucose metabolism and adipose tissue inflammation. **A:** The percentages of nuclear FLAG⁺ among F4/80⁺ cells in epididymal fat of *CNFoxo1^{LysM}* fed an HFD for 16 weeks. Counting of cells stained with anti-FLAG and anti-F4/80 are described in RESEARCH DESIGN AND METHODS. **B:** The percentages of nuclear Foxo1⁺ among F4/80⁺ cells in epididymal fat of control, *CNFoxo1^{LysM}* fed an NC, and *CNFoxo1^{LysM}* mice aged 20 weeks and fed an HFD for 16 weeks. Counting of cells stained with anti-F4/80 and anti-FOXO1 are described in RESEARCH DESIGN AND METHODS. Values are means \pm SEM of eight mice in each genotype. * $P < 0.005$ and ** $P < 0.05$ (one-factor ANOVA). **C:** Body weight (BW) of control and *CNFoxo1^{LysM}* mice fed an HFD. Data are means \pm SEM of 18–20 mice in each genotype. * $P < 0.05$ (two-way repeated-measures ANOVA with an ad hoc multiple comparison method [Fisher LSD test] of control vs. *CNFoxo1^{LysM}* mice after 8 weeks of HFD). **D:** IPGTT of control (open circle) and *CNFoxo1^{LysM}* mice fed an HFD. Data are means \pm SEM of 20–25 mice in each genotype. **E:** Comparison of AUC in control and *CNFoxo1^{LysM}* mice during IPGTT. Data are means \pm SEM of 20–25 mice in each genotype. * $P < 0.05$ (two-way repeated-measures ANOVA with Fisher LSD test of control vs. *CNFoxo1^{LysM}* mice). **F:** Insulin secretion of control (open circle) and *CNFoxo1^{LysM}* mice during IPGTT. Data are means \pm SEM of 20–25 mice in each genotype. * $P < 0.05$ (two-way repeated-measures ANOVA with Fisher LSD test of control vs. *CNFoxo1^{LysM}* mice). **G:** ITT of control (open circle) and *CNFoxo1^{LysM}* mice. Data are means \pm SEM of 20–25 mice in each genotype. * $P < 0.01$ and ** $P < 0.05$ (two-way repeated-measures ANOVA with Fisher LSD test of control vs. *CNFoxo1^{LysM}* mice). **H:** CLSs in epididymal fats were quantified from eight different fields per mouse and presented as number of CLSs per field. Data are means \pm SEM of 9–10 mice in each genotype. * $P < 0.05$ (one-factor ANOVA of control vs. *CNFoxo1^{LysM}* mice). **I:** Expression of F4/80 and CD11c and CD206 in cells of the SVF of epididymal fat from control and *CNFoxo1^{LysM}* mice fed an HFD for 16 weeks as assessed by flow cytometry. **J:** The percentages of F4/80⁺, F4/80⁺CD11c⁺CD206⁺, and F4/80⁺CD11c⁺CD206⁻ cells within the viable SVF from control and *CNFoxo1^{LysM}* 20- to 24-week-old mice fed an HFD for 16 weeks. The percentages of cell population among total SVF cells were calculated in each experiment. Data are means \pm SEM of fold change of control mice in each genotype ($n = 3$) analyzed in three independent experiments. * $P < 0.05$ (one-factor ANOVA of control vs. *CNFoxo1^{LysM}* mice).

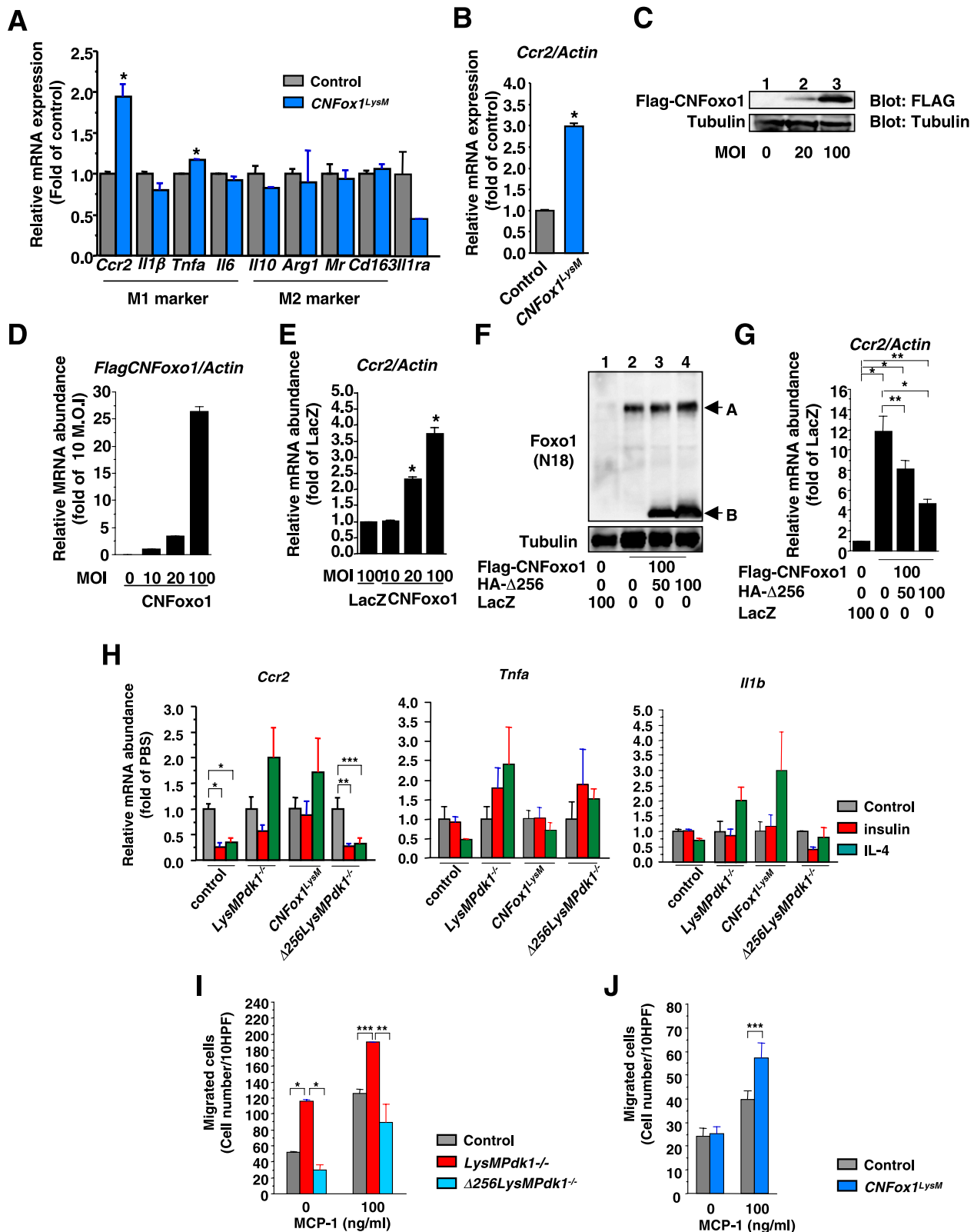


FIG. 5. Foxo1 increases migration capacity by inducing *Ccr2* expression. **A:** Expression of genes specific for M1 (*Ccr2*, *Il1b*, *Tnfa*, and *Il6*) or M2 (*Il10*, *Arg1*, *Mr*, and *Cd163*) phenotype of cells of the SVF from control and *CNFoxo1^{LysM}* mice fed an HFD for 16 weeks. Values were normalized to β -actin expression and represent the means \pm SEM of 8–10 mice per genotype. $*P < 0.05$ (one-factor ANOVA of control vs. *CNFoxo1^{LysM}* mice). **B:** Expression of *Ccr2* in ATMs sorted from the SVF of epididymal fat from control and *CNFoxo1^{LysM}* mice fed an HFD for 16 weeks. Values were normalized to β -actin expression and represent the means \pm SEM of three mice per genotype. $*P < 0.05$ (one-factor ANOVA of control vs. *CNFoxo1^{LysM}* mice). **C:** Flag-CNFoxo1 protein expression was detected in RAW264.7 cells. Nontransduced RAW264.7 cells (lane 1); RAW264.7 cells transduced with adenovirus encoding CNFoxo1 at 20 and 100 MOI (lanes 2 and 3, respectively). Western blot of cell lysates using anti-tubulin antibody (bottom). **D:** Expression of *Flag-CNFoxo1* gene in RAW264.7 cells transduced with adenoviruses encoding CNFoxo1 at the indicated MOI. **E:** Real-time PCR to determine *Ccr2* expression in RAW264.7 cells transduced with adenovirus encoding LacZ or CNFoxo1 at the indicated

and tissue weights of *CNFOxo1^{LysM}* mice were similar to those of control mice. However, adipocyte size in the epididymal fat of *CNFOxo1^{LysM}* mice tended to be larger than that in control mice (Fig. 4C and Supplementary Fig. 8A–C). Although, on the HFD, *CNFOxo1^{LysM}* and control mice exhibited similar glucose tolerance (Fig. 4D), the AUC of the IPGTT was significantly increased in *CNFOxo1^{LysM}* compared with control mice (Fig. 4E). Furthermore, the *CNFOxo1^{LysM}* mice exhibited significantly increased insulin secretion and decreased insulin sensitivity (Fig. 4F and G). These data suggest that the CNFOxo1 in ATMs caused insulin resistance.

M1 macrophage population was increased in *CNFOxo1^{LysM}* mice. Adipocyte size and CLS density exhibit a positive correlation (32,36). Indeed, under HFD conditions, *CNFOxo1^{LysM}* mice had a significantly higher number of CLSs in epididymal fat than control mice (Fig. 4H). Phenotypic analysis of ATMs revealed significantly more F4/80⁺ cells in the SVF of *CNFOxo1^{LysM}* mice compared with control mice (Fig. 4I and J). Further analysis showed that *CNFOxo1^{LysM}* mice had a significantly higher percentage of F4/80⁺CD11c⁺CD206⁻ and F4/80⁺CD11c⁻CD206⁺ cells compared with control mice (Fig. 4I and J). These data suggest that the *CNFOxo1^{LysM}* mice have increased numbers of macrophages in adipose tissues under HFD conditions.

CNFOxo1-induced *Ccr2* gene expression. To investigate how CNFOxo1 increased the M1 macrophage subpopulation in adipose tissue, we analyzed gene expression in the SVF of epididymal fat from mice fed an HFD. Real-time PCR demonstrated that *CNFOxo1^{LysM}* mice expressed significantly higher levels of *Ccr2* and *Tnfa* mRNAs than control mice (Fig. 5A). Furthermore, the level of *Ccr2* expression in F4/80⁺CD11c⁺CD206⁻ cells was significantly increased in *CNFOxo1^{LysM}* mice compared with control mice (Fig. 5B). To examine whether CNFOxo1 directly induces *Ccr2* expression, we infected RAW264.7 cells with an adenovirus encoding β -galactosidase or CNFOxo1. Overexpression of CNFOxo1 in RAW264.7 cells significantly increased endogenous *Ccr2* expression (Fig. 5C–E). These data suggest that the overexpression of CNFOxo1 in ATMs increased *Ccr2* expression.

Next, we investigated whether $\Delta 256$ Foxo1 could block Foxo1-induced *Ccr2* expression. We cotransduced RAW264.7 cells with adenoviruses that encoded Flag-CNFOxo1 and HA- $\Delta 256$ Foxo1. We found that the presence of $\Delta 256$ Foxo1 inhibited the expression of endogenous *Ccr2* in a dose-dependent manner (Fig. 5F and G). These data indicate and confirm that the $\Delta 256$ Foxo1 construct had a dominant negative effect on Foxo1-induced *Ccr2* expression.

Insulin- and IL-4-inhibited *Ccr2* gene expression. To determine whether Foxo1 regulation of *Ccr2* expression

was involved in insulin signaling, we tested whether insulin or IL-4 inhibited *Ccr2* expression in a Foxo1-dependent manner. Both insulin and IL-4 could significantly inhibit *Ccr2* expression in BMDMs from control and $\Delta 256$ *LysMPdk1^{-/-}* mice but not in BMDMs from *LysMPdk1^{-/-}* and *CNFOxo1^{LysM}* mice (Fig. 5H). In contrast, insulin and IL-4 did not affect expression of other genes specifically expressed in M1 macrophages, including *Tnfa* and *Il1b* (Fig. 5H). These data indicate that Foxo1-induced *Ccr2* expression was regulated by both insulin and IL-4.

Pdk1 deletion or CNFOxo1 expression enhanced macrophage migration. To analyze the functional effects of Pdk1 deficiency in macrophages, we performed transwell migration assays with BMDMs. Pdk1-deficient BMDMs exhibited significantly more migration than BMDMs from control and $\Delta 256$ *LysMPdk1^{-/-}* mice (Fig. 5I). Furthermore, BMDMs from *CNFOxo1^{LysM}* mice exhibited significantly increased MCP-1-stimulated migration capacity compared with control BMDMs (Fig. 5J). These data confirm that a Pdk1 deficiency and/or Foxo1 activation in macrophages resulted in increased migration as a result of increased expression of *Ccr2*.

Characterization of the Foxo1 response element within the *Ccr2* promoter. To characterize the Foxo1 response element (FRE) in the *Ccr2* promoter, we constructed different versions of the mouse *Ccr2* promoter by progressively deleting portions of the upstream region. The transcriptional activity of each mutant promoter in response to CNFOxo1 binding was examined in HEK293T cells (Fig. 6A). *Ccr2* promoters with deletions up to -291 nucleotides (nt) responded to Foxo1 transactivation. However, further deletions, up to -208 nt, completely abolished transcription of the reporter (Fig. 6A). Thus, the FRE was confined to a small nucleotide region between -291 and -208 in the mouse *Ccr2* promoter. Consistent with this observation, the promoter region contained several putative Foxo response elements (FREs), including GTAAAT from -254 to -249 nt and AAACA from -215 to -211 nt (Fig. 6A). It is interesting that the former region is conserved among human, mouse, and rat *Ccr2* promoters (Supplementary Fig. 9). To confirm this finding, we generated one additional truncated mutant promoter (237*Ccr2*), which had the latter FRE but not the former. The 237*Ccr2* promoter did not respond to Foxo1 induction. These data suggest that the AAACA sequence from -215 to -211 was unnecessary for Foxo1 activation of the *Ccr2* promoter. We also generated two additional mutant *Ccr2* promoters, one harboring nucleotide substitutions between -254 and -249 (254mut) and one with substitutions between -215 and -211 (215mut). Foxo1 induced transcription from the 215mut but not from the 254mut *Ccr2* promoter (Fig. 6A). These data suggest that the GTAAAT

MOI. The cells were transduced, incubated in complete medium, and harvested 48 h after transduction. Data (mean \pm SEM) are from three independent experiments and normalized to the amount of β -actin mRNA, expressed as relative to the corresponding LacZ value. * $P < 0.05$ (one-factor ANOVA of cells transduced with LacZ vs. CNFOxo1 at 20 or 100 MOI). **F:** Expression of Flag CNFOxo1 and HA- $\Delta 256$ Foxo1 at indicated MOI in RAW264.7 cells. Western blot using anti-Foxo1 (N18) antibody, which recognizes the NH₂ terminus of Foxo1 (top). Arrows A and B indicate Flag-CNFOxo1 and HA- $\Delta 256$ Foxo1, respectively. **G:** The effects of HA- $\Delta 256$ Foxo1 on Flag-CNFOxo1-induced *Ccr2* expression in RAW264.7 cells. Data are means \pm SEM from three independent experiments and are expressed as the fold change from endogenous *Ccr2* expression in RAW264.7 cells transduced with an adenovirus encoding LacZ. * $P < 0.005$ and ** $P < 0.05$ (one-factor ANOVA of cells transduced with LacZ vs. Flag-CNFOxo1 at MOI 100 and cells transduced with Flag-CNFOxo1 at MOI 100 vs. HA- $\Delta 256$ Foxo1 at MOI 50 and 100). **H:** Expression of genes *Ccr2*, *Tnfa*, and *Il1b* of BMDM from the indicated genotypes. Cells were cultured for 6 days in the presence of PBS, insulin (100 nmol/L), or IL-4 (100 ng/mL). Values were normalized to β -actin expression and represent the means \pm SEM of fold of PBS in each genotype (8–10 mice per genotype). * $P < 0.005$ (one-factor ANOVA of PBS vs. insulin or IL-4 in control mice), ** $P < 0.01$ (one-factor ANOVA of PBS vs. insulin in $\Delta 256$ *LysMPdk1^{-/-}* mice), and *** $P < 0.05$ (one-factor ANOVA of PBS vs. IL-4 in $\Delta 256$ *LysMPdk1^{-/-}* mice). **I and J:** Migration of BMDM from control, *LysMPdk1^{-/-}*, and $\Delta 256$ *LysMPdk1^{-/-}* mice (I) and from control and *CNFOxo1^{LysM}* mice (J) through a gelatin matrix was analyzed using a transwell migration assay at the indicated concentration of MCP-1. Data are means \pm SEM of cell numbers per 10 high power fields (HPFs) from three independent experiments. * $P < 0.005$ (one-factor ANOVA of *LysMPdk1^{-/-}* vs. control or $\Delta 256$ *LysMPdk1^{-/-}* mice at basal condition), ** $P < 0.01$ (one-factor ANOVA of *LysMPdk1^{-/-}* vs. $\Delta 256$ *LysMPdk1^{-/-}* mice at 100 ng/mL of MCP-1), and *** $P < 0.05$ (one-factor ANOVA of *LysMPdk1^{-/-}* vs. control mice and of control vs. *CNFOxo1^{LysM}* mice at 100 ng/mL of MCP-1).

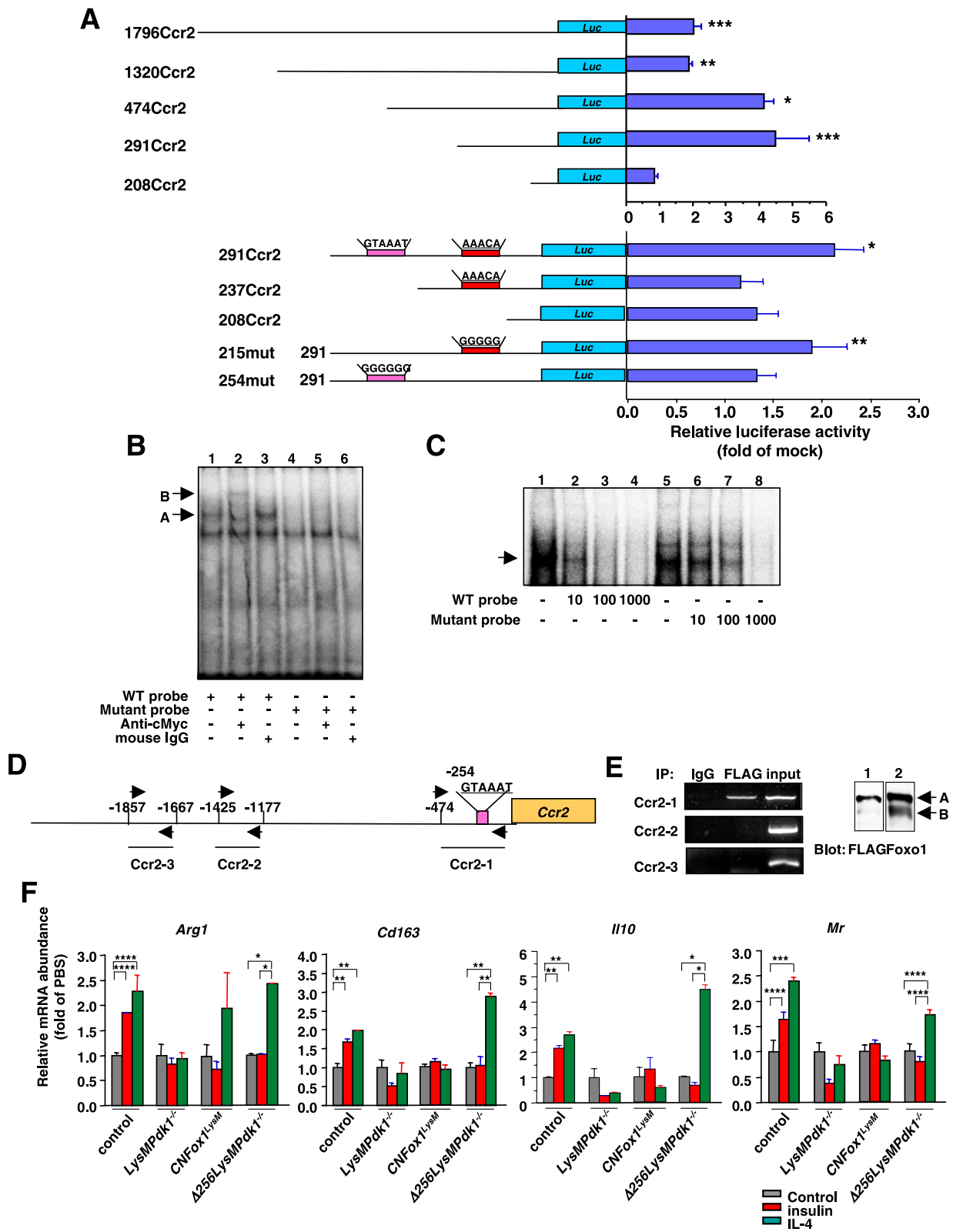


FIG. 6. *Ccr2* as a target gene of Foxo1 and the effects of insulin or IL-4 on genes for M2 signature. **A:** Effect of Foxo1 on *Ccr2* promoter activity. Data were obtained from 10 experiments and are represented as means \pm SEM of fold change from mock vector-transfected activity. * $P < 0.001$, ** $P < 0.005$, and *** $P < 0.05$ (one-factor ANOVA of cells transfected with pCMV5/cMyc and pCVM5/cMyc-CNFoxo1 vector). **B:** EMSA of Foxo1 binding to DNA. The DNA probe was derived from a 31-base pair DNA covering the consensus Foxo1 binding site (-267/-237 nt) of the mouse *Ccr2* promoter (lanes 1-3). A mutant DNA with an altered Foxo1 binding motif was used as a control (lanes 4-6). The position of the slowed complex is indicated as A, and the supershifted complex is indicated as B. **C:** Oligonucleotide probes corresponding to the Foxo1 binding site of the *Ccr2* promoter were incubated with nuclear extracts in the absence or presence of increasing amounts of unlabeled wild-type (lanes 1-4) or mutant oligonucleotide (lanes 5-8). **D:** Mouse *Ccr2* promoter and primer pairs used in ChIP assay. The magenta box indicates a consensus Foxo1 binding site. **E:** ChIP assays of RAW264.7 cells transduced with an adenovirus encoding CNFoxo1 and harvested 36 h after transduction (left). The PCR primers amplified the mouse *Ccr2* promoter sequence as shown in Fig. 5G. PCR reactions with total input chromatin are shown as control.

sequence from -254 to -249 nt in the mouse *Ccr2* promoter was the functional FRE.

Association of Foxo1 with the *Ccr2* promoter. To examine the ability of this putative FRE to bind Foxo1, we conducted an EMSA. Foxo1 caused significant retardation of the FRE DNA (Fig. 6B, lane 1). Inclusion of the anti-cMyc antibody resulted in a supershifted DNA band (Fig. 6B, lane 2). The same EMSA was performed using a mutant DNA containing five base substitutions within the FRE motif as a control. Alterations in the consensus FRE motif abrogated its ability to bind Foxo1 (Fig. 6B, lane 4). Incubating nuclear extracts from cells expressing cMyc-tagged Foxo1 with a probe encoding the 31-base pair FRE DNA sequence yielded a slower complex that was competed out by excess cold probe (Fig. 6C, lanes 1–4) but not mutant probe (Fig. 6C, lanes 5–8).

We performed a ChIP assay to determine the association between Foxo1 and the *Ccr2* promoter in RAW264.7 cells. Because of low levels of Foxo1 expression in RAW264.7 cells, we transduced cells with adenovirus encoding CNFoxo1. Using primers flanking the FRE motif within the *Ccr2* promoter (Fig. 6D), we detected a sequence-specific DNA corresponding to the proximal region (-474/9 nt) of the *Ccr2* promoter in immunoprecipitates obtained with anti-FLAG antibody (Fig. 6E). We also performed PCR analysis using a pair of off-target primers flanking distal regions (-1857/-1667 and -1425/-1177 nt). No specific DNA was amplified in the immunoprecipitates using normal mouse IgG or anti-FLAG antibody (Fig. 6E). These data confirm that Foxo1 directly binds the *Ccr2* promoter and that *Ccr2* is a target gene of Foxo1.

The Pdk1-Foxo1 pathway plays a role in alternative macrophage activation. To determine whether the Pdk1-Foxo1 pathway was essential for alternative activation of macrophages, we analyzed macrophage signatures in insulin- or IL-4-stimulated BMDMs from control, *LysMPdk1*^{-/-}, *CNFoxo1*^{LysM}, and $\Delta 256$ *LysMPdk1*^{-/-} mice. The signature genes, including *Arg1*, *Cd163*, *Il10*, and *Mr*, were significantly induced by insulin or IL-4 in BMDMs from control mice (Fig. 6F). In contrast, Pdk1 deficiency or constitutive Foxo1 activation completely abolished insulin- or IL-4-stimulated induction of the genes necessary for alternative macrophage activation (Fig. 6F). It is interesting that the expression of transactivation-defective ($\Delta 256$) Foxo1 rescued IL-4-induced, but not insulin-induced, gene expression (Fig. 6F). These data indicate that the Pdk1-Foxo1 pathway was required for the activation of macrophages via the alternative pathway.

A transactivation-defective ($\Delta 256$) Foxo1 partially protected against diet-induced insulin resistance. To determine whether blocking Foxo1 transactivation by expressing $\Delta 256$ Foxo1 in ATMs would alleviate insulin resistance, we compared glucose homeostasis and insulin sensitivity in wild-type and $\Delta 256$ *Foxo1*^{LysM} mice fed an HFD for 24 weeks. We observed no differences in body weight, glucose tolerance, or insulin secretion between genotypes (Fig. 7A–C). Furthermore, the $\Delta 256$ *Foxo1*^{LysM} mice showed a weak but significant improvement in insulin sensitivity compared with wild-type mice (Fig. 7D and E).

After a 24-week HFD, $\Delta 256$ *Foxo1*^{LysM} and wild-type mice had similar proportions of F4/80⁺, F4/80⁺CD11c⁺CD206⁻, and F4/80⁺CD11c⁻CD206⁺ cells in adipose tissues (Fig. 7F). Moreover, in epididymal fat, no differences were observed in the gene expression profiles of M1 macrophages, including *Ccr2*, *Il1b*, *Tnfa*, and *Il6*. However, there was a significant increase in *Arg1* expression in $\Delta 256$ *Foxo1*^{LysM} compared with control mice (Fig. 7G). Taken together, these data show that overexpression of $\Delta 256$ Foxo1 in macrophages did not prevent glucose intolerance, but it did partially alleviate insulin resistance.

DISCUSSION

In the current study, we demonstrate that Pdk1 in ATMs inhibits recruitment of M1 macrophages into adipose tissues, while Foxo1 antagonizes these processes. These findings suggest that the Pdk1-Foxo1 signaling pathway in ATMs is important for regulation of chronic inflammation and insulin sensitivity in vivo (Fig. 8).

The key finding of the current study was that Foxo1 targeted *Ccr2* expression in macrophages. *Ccr2* is the primary receptor for Mcp1/Ccl2, a member of the chemokine family of proteins. *Ccr2* is expressed on circulating monocytes and ATMs, where it serves as a crucial monocyte recruitment factor by directing macrophages to sites of injury and inflammation. Furthermore, *Ccr2* is important in the regulation of insulin sensitivity in vivo. Obesity increases the production of Ccl2 in adipose tissues, which leads to an accumulation of Ccl2-bound macrophages. When recruited macrophages are classically activated, they secrete proinflammatory cytokines, which leads to insulin resistance in various insulin-responsive tissues (2). Indeed, *Ccr2* deletion ameliorated insulin resistance in HFD-induced insulin resistance (37). Therefore, our observation of increased *Ccr2* expression in SVF M1 macrophages in *LysMPdk1*^{-/-} and *CNFoxo1*^{LysM} mice was an important cue that insulin resistance had developed. Thus, the current study directly demonstrates that ATM Foxo1 played a pivotal role in regulating insulin sensitivity in vivo.

Nuclear accumulation of Foxo1 suddenly increased at 24 weeks of HFD, although phosphorylation of Pdk1 was not changed. These findings suggest that another signaling pathway may be involved in subcellular localization of Foxo1 in ATMs. One of the candidates is MST1, which mediates oxidative stress, phosphorylates FOXO proteins at a conserved site within the forkhead domain, disrupts their interaction with 14-3-3 proteins, and promotes FOXO nuclear translocation (27). Furthermore, JNK is known to phosphorylate and activate MST1 (30). HFD increased oxidative stress (18), leading to activation of JNK, MST1, and nuclear accumulation of Foxo1 (27). Of interest, we observed that H₂O₂ significantly increased at 24 weeks of HFD and that phosphorylation of MST1 also significantly increased at the same time. Therefore, oxidative stress in HFD may contribute to nuclear accumulation and activation of Foxo1. The findings suggest that nuclear accumulation of Foxo1 contributes to recruitment of M1 macrophages into adipose tissue during HFD.

Western blotting of transduced CNFoxo1 using anti-FLAG (lane 1) and anti-Foxo1 (lane 2) antibodies (right). The position of CNFoxo1 is indicated as A, and endogenous Foxo1 is indicated as B. F: Expression of genes *Arg1*, *Cd163*, *Il10*, and *Mr* of BMDM from the indicated genotypes. Cells were cultured for 2 days in the presence of PBS (control), insulin (100 nmol/L), or IL-4 (100 ng/mL). Values were normalized to β -actin expression and represent the means \pm SEM of fold of PBS in each genotype (8–10 mice per genotype). **P* < 0.001, ***P* < 0.005, ****P* < 0.01, and *****P* < 0.05 (one-factor ANOVA among the indicated genotypes). WT, wild-type.

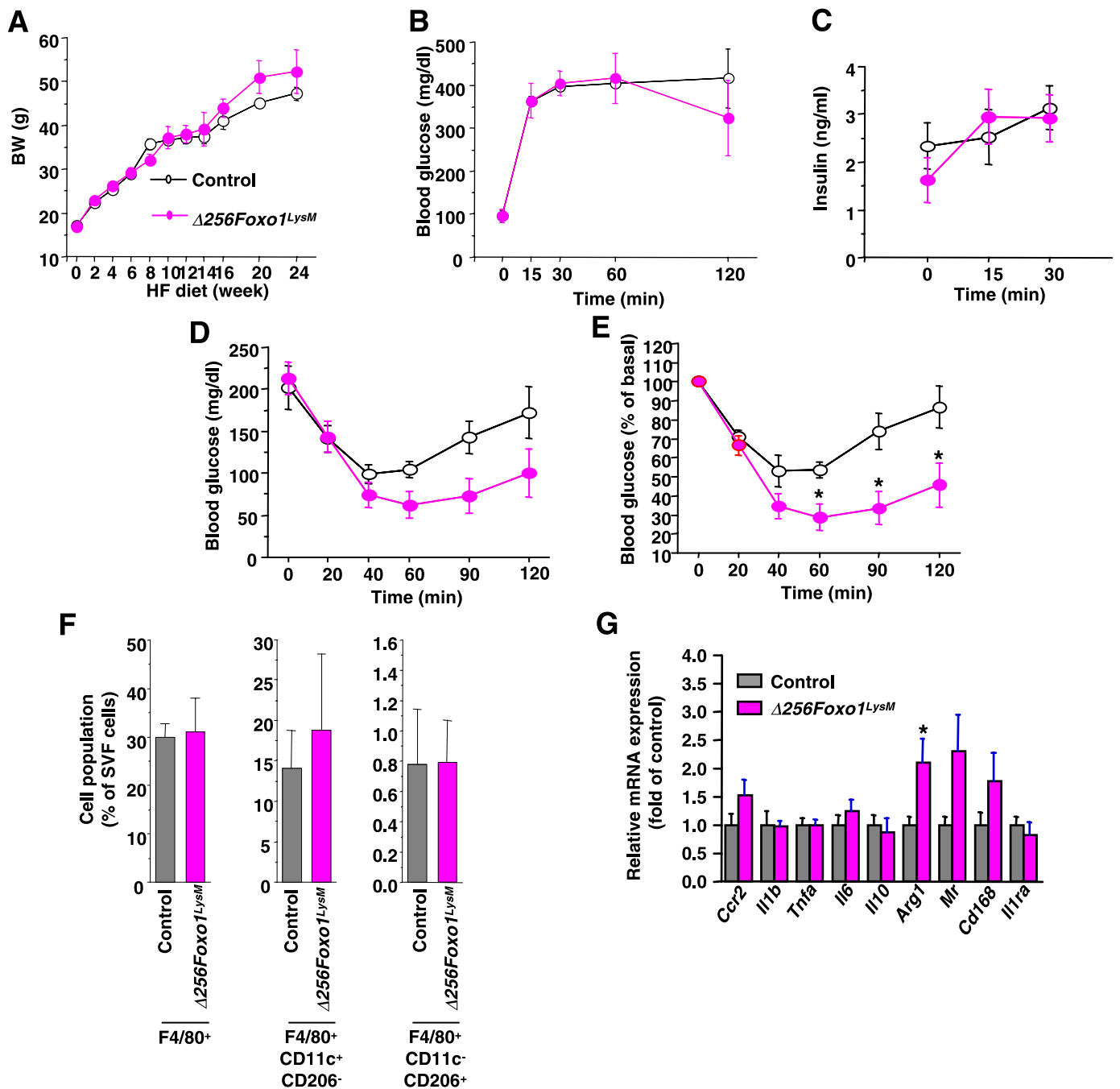


FIG. 7. A transactivation-defective ($\Delta 256$) Foxo1 partially protected against diet-induced insulin resistance. **A:** Body weight (BW) of control and $\Delta 256Foxo1^{LysM}$ mice fed an HFD. Data are means + SEM of 20 mice in each genotype. **B:** IPGTT of control (open circle) and $\Delta 256Foxo1^{LysM}$ (magenta circle) mice fed an HFD. Data are means + SEM of 20 mice in each genotype. **C:** Insulin secretion of control (open circle) and $\Delta 256Foxo1^{LysM}$ (magenta circle) mice during IPGTT. Data are means + SEM of 20 mice in each genotype. **D** and **E:** ITT of control (open circle) and $\Delta 256Foxo1^{LysM}$ (magenta circle) mice. Data are means + SEM of 20 mice in each genotype as absolute glucose values (**D**) and the percentages of basal values (**E**). * $P < 0.05$ (two-way repeated-measures ANOVA with an ad hoc multiple comparison method [Fisher's LSD test] of control vs. $\Delta 256Foxo1^{LysM}$ mice). **F:** The percentages of F4/80⁺, F4/80⁺CD11c⁺CD206⁻, and F4/80⁺CD11c⁻CD206⁺ cells within the viable SVF from 20- to 24-week-old mice of control and $\Delta 256Foxo1^{LysM}$ mice. Data are means + SEM of 6 mice in each genotype analyzed in three independent experiments. **G:** Expression of genes in the epididymal fat of control and $\Delta 256Foxo1^{LysM}$ mice. Values were normalized to β -actin expression and represent the means + SEM of 8–10 mice per genotype. * $P < 0.05$ (one-factor ANOVA of control vs. $\Delta 256Foxo1^{LysM}$ mice).

However, we observed that expression of $\Delta 256Foxo1$ just partially protected against diet-induced insulin resistance and could not rescue *Ccr2* expression in mice fed an HFD for 24 weeks. Furthermore, the current study demonstrates that nuclear localization of Foxo1 started to occur at 24 weeks of HFD. Therefore, it is possible that nuclear localization of Foxo1 plays a role specifically in the late progression of

diet-induced insulin resistance. From the current study, nuclear accumulation of Foxo1 in ATMs is only 40–45% of all F4/80⁺ at 24 weeks of HFD, which means that an HFD cannot activate Foxo1 in ATMs completely. In contrast, the percentages of nuclear Foxo1 in ATMs of *LysMPdk1*^{-/-} and *CNFoxo1*^{LysM} fed an HFD are ~70%. Therefore, the effect of loss of transactivation of Foxo1 on *Ccr2* expression in an

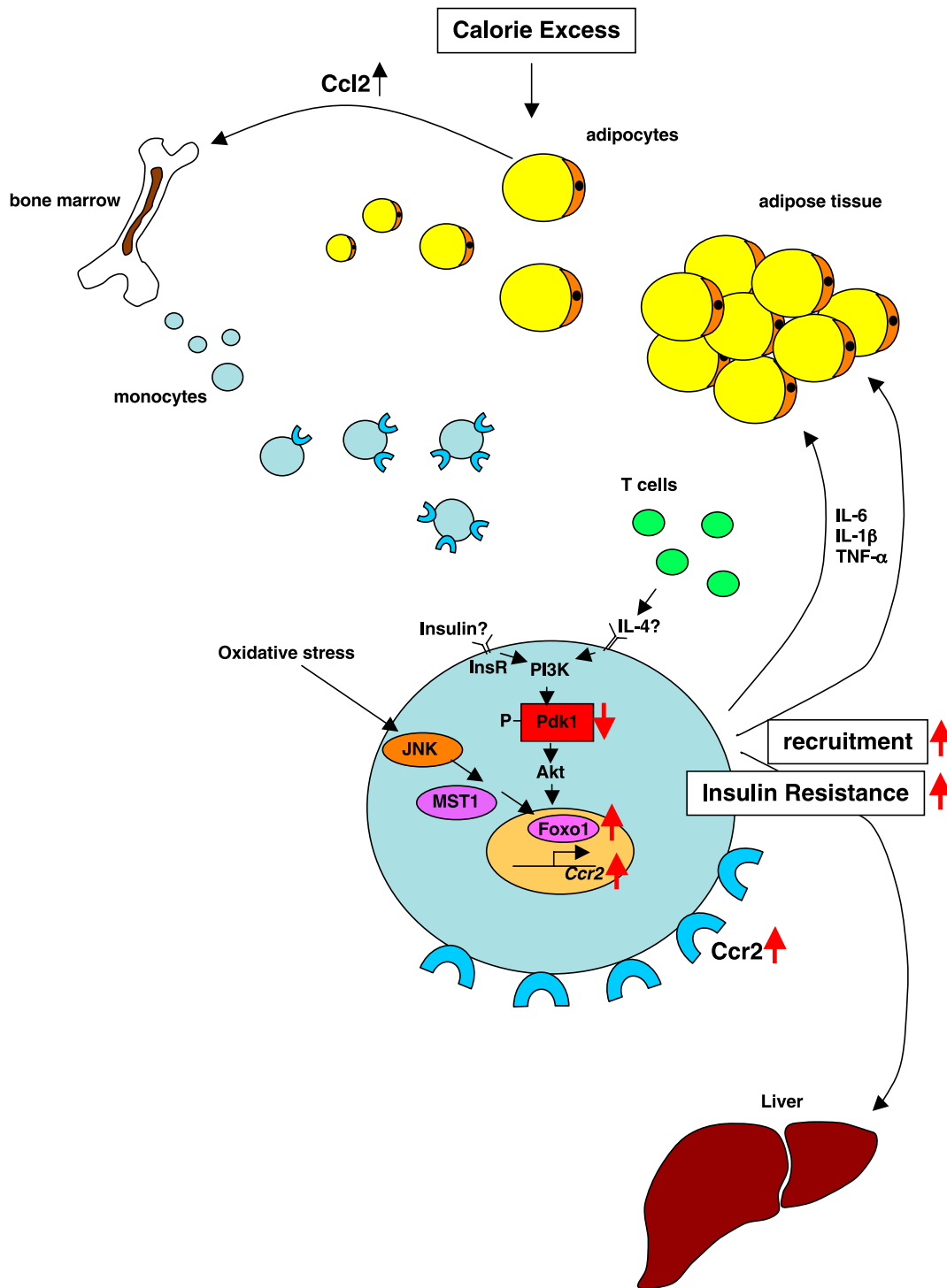


FIG. 8. Control of ATM function by Pdk1-Foxo1 pathway. Pdk1 is regulated by not only insulin but also cytokines, including IL-4, which is secreted from CD4⁺ T cells or regulatory T cells. Furthermore, Foxo1 is regulated by not only Pdk1 but also oxidative stress through JNK and MST1. Phosphorylation of Pdk1 gradually declined during the HFD, but oxidative stress suddenly increased at the prolonged HFD, which is consistent with the time for the increased nuclear accumulation of Foxo1 in ATMs. Foxo1 directly regulates the expression of Ccr2, which upregulates the recruitment of macrophages in adipose tissue. PI3K, phosphatidylinositol 3-kinase.

HFD is small compared with *LysMPdk1*^{-/-} mice. Alternatively, nuclear Foxo1 in myeloid cells may promote insulin resistance by other mechanisms than its role in the control of *Ccr2* gene expression. Furthermore, the *CNFoxo1*^{LysM} mice fed an NCD did not exhibit insulin resistance, while *LysMPdk1*^{-/-} mice exhibited insulin resistance. These findings suggest that Foxo1 per se is not sufficient to

cause HFD-induced insulin resistance, although Foxo1 may enhance the negative effect of an HFD on insulin sensitivity.

Our results provide direct evidence for the notion that ATM cell autonomous Pdk1-Foxo1 signaling regulates adipose tissue inflammation and insulin sensitivity in vivo. This finding may suggest a new target for pharmacological

intervention that could lead to novel therapeutic strategies for treating insulin resistance and type 2 diabetes.

ACKNOWLEDGMENTS

This work was supported by a grant from Nippon Boehringer Ingelheim Co., Ltd. to H.I. and a grant from Keio University Grant-in-Aid for Encouragement of Young Medical Scientists to Y.K. No other potential conflicts of interest relevant to this article were reported.

Y.K. researched data. J.N. conceived the hypothesis, designed and researched data, supervised the analyses, and wrote the manuscript. N.W., S.F., K.I., R.S., Y.H., and K.T. researched data. M.K. and T.N. generated and provided tissue-specific *Pdk1* knockout mice. A.Y. provided *LysMCre* mice and helpful discussion regarding experiments. M.O. researched data and assisted with data interpretation. H.I. supervised all experiments and assisted with preparation of the manuscript. J.N. is the guarantor of this work and, as such, had full access to all the data in the study and takes responsibility for the integrity of the data and the accuracy of the data analysis.

The authors thank Takahito Kaji (Training Department, Customer & Commercial Excellence, MSD K.K.) for analysis of data by two-way repeated-measures ANOVA.

REFERENCES

- Qatanani M, Lazar MA. Mechanisms of obesity-associated insulin resistance: many choices on the menu. *Genes Dev* 2007;21:1443–1455
- Olefsky JM, Glass CK. Macrophages, inflammation, and insulin resistance. *Annu Rev Physiol* 2010;72:219–246
- Saltiel AR, Kahn CR. Insulin signalling and the regulation of glucose and lipid metabolism. *Nature* 2001;414:799–806
- Welham MJ, Bone H, Levings M, et al. Insulin receptor substrate-2 is the major 170-kDa protein phosphorylated on tyrosine in response to cytokines in murine lymphohemopoietic cells. *J Biol Chem* 1997;272:1377–1381
- Frittitta L, Grasso G, Munguira ME, Vigneri R, Trischitta V. Insulin receptor tyrosine kinase activity is reduced in monocytes from non-obese normoglycaemic insulin-resistant subjects. *Diabetologia* 1993;36:1163–1167
- Zoppini G, Galante P, Zardini M, Muggeo M. Phosphotyrosine protein profiles in monocytes after insulin and IGF-1 stimulation. *Eur J Clin Invest* 1994;24:275–278
- Liang CP, Han S, Okamoto H, et al. Increased CD36 protein as a response to defective insulin signaling in macrophages. *J Clin Invest* 2004;113:764–773
- Han S, Liang CP, DeVries-Seimon T, et al. Macrophage insulin receptor deficiency increases ER stress-induced apoptosis and necrotic core formation in advanced atherosclerotic lesions. *Cell Metab* 2006;3:257–266
- Senokuchi T, Liang CP, Seimon TA, et al. Forkhead transcription factors (FoxOs) promote apoptosis of insulin-resistant macrophages during cholesterol-induced endoplasmic reticulum stress. *Diabetes* 2008;57:2967–2976
- Hashimoto N, Kido Y, Uchida T, et al. Ablation of PDK1 in pancreatic beta cells induces diabetes as a result of loss of beta cell mass. *Nat Genet* 2006;38:589–593
- Iskandar K, Cao Y, Hayashi Y, et al. PDK1/FoxO1 pathway in POMC neurons regulates Pomc expression and food intake. *Am J Physiol Endocrinol Metab* 2010;298:E787–E798
- Su D, Coudriet GM, Hyun Kim D, et al. FoxO1 links insulin resistance to proinflammatory cytokine IL-1 β production in macrophages. *Diabetes* 2009;58:2624–2633
- Fan W, Morinaga H, Kim JJ, et al. FoxO1 regulates Tlr4 inflammatory pathway signalling in macrophages. *EMBO J* 2010;29:4223–4236
- Clausen BE, Burkhardt C, Reith W, Renkawitz R, Förster I. Conditional gene targeting in macrophages and granulocytes using *LysMcre* mice. *Transgenic Res* 1999;8:265–277
- Nakae J, Cao Y, Oki M, et al. Forkhead transcription factor FoxO1 in adipose tissue regulates energy storage and expenditure. *Diabetes* 2008;57:563–576
- Fujisaka S, Usui I, Bukhari A, et al. Regulatory mechanisms for adipose tissue M1 and M2 macrophages in diet-induced obese mice. *Diabetes* 2009;58:2574–2582
- Nakae J, Biggs WH 3rd, Kitamura T, et al. Regulation of insulin action and pancreatic beta-cell function by mutated alleles of the gene encoding forkhead transcription factor Foxo1. *Nat Genet* 2002;32:245–253
- Furukawa S, Fujita T, Shimabukuro M, et al. Increased oxidative stress in obesity and its impact on metabolic syndrome. *J Clin Invest* 2004;114:1752–1761
- Odegaard JI, Ricardo-Gonzalez RR, Goforth MH, et al. Macrophage-specific PPAR γ controls alternative activation and improves insulin resistance. *Nature* 2007;447:1116–1120
- Mauer J, Chaurasia B, Plum L, et al. Myeloid cell-restricted insulin receptor deficiency protects against obesity-induced inflammation and systemic insulin resistance. *PLoS Genet* 2010;6:e1000938
- Nakae J, Kitamura T, Silver DL, Accili D. The forkhead transcription factor Foxo1 (Fkhr) confers insulin sensitivity onto glucose-6-phosphatase expression. *J Clin Invest* 2001;108:1359–1367
- Nakae J, Cao Y, Daitoku H, et al. The LXXLL motif of murine forkhead transcription factor FoxO1 mediates Sirt1-dependent transcriptional activity. *J Clin Invest* 2006;116:2473–2483
- Kubota N, Kubota T, Itoh S, et al. Dynamic functional relay between insulin receptor substrate 1 and 2 in hepatic insulin signaling during fasting and feeding. *Cell Metab* 2008;8:49–64
- Nakae J, Kitamura T, Kitamura Y, Biggs WH 3rd, Arden KC, Accili D. The forkhead transcription factor Foxo1 regulates adipocyte differentiation. *Dev Cell* 2003;4:119–129
- Casamayor A, Morrice NA, Alessi DR. Phosphorylation of Ser-241 is essential for the activity of 3-phosphoinositide-dependent protein kinase-1: identification of five sites of phosphorylation in vivo. *Biochem J* 1999;342:287–292
- Accili D, Arden KC. FoxOs at the crossroads of cellular metabolism, differentiation, and transformation. *Cell* 2004;117:421–426
- Lehtinen MK, Yuan Z, Boag PR, et al. A conserved MST-FOXO signaling pathway mediates oxidative-stress responses and extends life span. *Cell* 2006;125:987–1001
- Choi J, Oh S, Lee D, et al. Mst1-FoxO signaling protects naïve T lymphocytes from cellular oxidative stress in mice. *PLoS ONE* 2009;4:e8011
- Yuan Z, Lehtinen MK, Merlo P, Villén J, Gygi S, Bonni A. Regulation of neuronal cell death by MST1-FOXO1 signaling. *J Biol Chem* 2009;284:11285–11292
- Bi W, Xiao L, Jia Y, et al. c-Jun N-terminal kinase enhances MST1-mediated pro-apoptotic signaling through phosphorylation at Serine 82. *J Biol Chem* 2010;285:6259–6264
- Nakae J, Barr V, Accili D. Differential regulation of gene expression by insulin and IGF-1 receptors correlates with phosphorylation of a single amino acid residue in the forkhead transcription factor FKHR. *EMBO J* 2000;19:989–996
- Murano I, Barbatelli G, Parisani V, et al. Dead adipocytes, detected as crown-like structures, are prevalent in visceral fat depots of genetically obese mice. *J Lipid Res* 2008;49:1562–1568
- Sauter NS, Schulthess FT, Galasso R, Castellani LW, Maedler K. The anti-inflammatory cytokine interleukin-1 receptor antagonist protects from high-fat diet-induced hyperglycemia. *Endocrinology* 2008;149:2208–2218
- Naito M. Macrophage differentiation and function in health and disease. *Pathol Int* 2008;58:143–155
- Hanisch UK, Kettenmann H. Microglia: active sensor and versatile effector cells in the normal and pathologic brain. *Nat Neurosci* 2007;10:1387–1394
- Weisberg SP, McCann D, Desai M, Rosenbaum M, Leibel RL, Ferrante AW Jr. Obesity is associated with macrophage accumulation in adipose tissue. *J Clin Invest* 2003;112:1796–1808
- Weisberg SP, Hunter D, Huber R, et al. CCR2 modulates inflammatory and metabolic effects of high-fat feeding. *J Clin Invest* 2006;116:115–124